Coupled cavities for motional ground-state cooling and strong optomechanical coupling

Yong-Chun Liu, Yun-Feng Xiao, Xingsheng Luan, Qihuang Gong, and Chee Wei Wong

Phys. Rev. A **91**, 033818 — Published 16 March 2015

DOI: 10.1103/PhysRevA.91.033818

Coupled cavities for motional ground state cooling and strong optomechanical coupling

Yong-Chun Liu[1], Yun-Feng Xiao[1],* Xingsheng Luan[2], Qihuang Gong[1], and Chee Wei Wong[2]†
[1]*State Key Laboratory for Mesoscopic Physics and School of Physics, Peking University; Collaborative Innovation Center of Quantum Matter, Beijing 100871, P. R. China and*
[2]*Optical Nanostructures Laboratory, Columbia University, New York, NY 10027, USA*
(Dated: February 13, 2015)

Motional ground state cooling and quantum-coherent manipulation of mesoscopic mechanical systems are crucial goals in both fundamental physics and applied science. We demonstrate that the motional ground state can be achieved in the highly unresolved sideband regime, through coherent auxiliary cavity interferences. We further illustrate coherent strong Rabi coupling between indirectly-coupled and individually-optimized mechanical resonators and optical cavities through effective dark-mode interaction. The proposed approach provides a new platform for quantum manipulation of mesoscopic mechanical devices beyond the resolved sideband limit.

PACS numbers: 42.50.Wk, 07.10.Cm, 42.50.Lc

I. INTRODUCTION

Preparing mechanical quantum states free of thermal noise and with coherent manipulation are crucial goals in cavity optomechanics [1–6]. Recently significant efforts on motional ground state cooling have been mounted through dispersive coupling [7–15], along with recent theoretical efforts on dissipative coupling [16, 17], dynamic cooling [18–22], atom-assisted cooling [23–25] and external cavity cooling [26]. Quantum noise however sets a fundamental limit for backaction cooling, and current dispersive ground state cooling approaches must rely on the resolved sideband limit [27, 28], requiring a cavity linewidth smaller than the single harmonic oscillator level spacing. In parallel, interference phenomena have been observed in optomechanical systems [29–32], including a mechanical mode interacting with two optical modes [33–39], with the application of coherent frequency conversion [40, 41] and dark mode observations [42] in the weak optomechanical coupling regime. For coherent exchange between optical and mechanical modes [43–46], however, a dramatically large optomechanical coupling rate exceeding that of optical decoherence has been deemed necessary. Conventionally, this poses a serious requirement on the optical Q-factor, i.e., the good-cavity and resolved sideband limits.

Recently some approaches on ground state cooling in the unresolved sideband regime [5] have been proposed. The dissipative coupling mechanism [16, 17], parameter modulations [18–21] and hybrid system approaches [23–25, 47] are shown to be capable of loosening resolved sideband condition. However, experimental realization of these proposals are still difficult. Here we propose a practical coupled cavity system for both ground state cooling of mechanical resonators and strong optomechanical coupling in the highly unresolved sideband condition, without requiring the coupled cavities in the normal mode splitting regime. We harness the destructive quantum interference in the all-optical domain of the coupled cavity system to achieve these goals. We find that ground state cooling is realizable for a large range of cavity decay rates by coherently coupling to an auxiliary optical resonator or mode, which does not directly interact with the mechanical mode. We use effective dark-mode interaction model to analytically describe the system, and demonstrate quantum-coherent coupling between individually-optimized mechanical resonators and optical cavities. This not only allows quantum manipulation of massive mesoscopic mechanical devices with low frequencies, but also enables quantum effects in a general platform with optimized optical and mechanical properties.

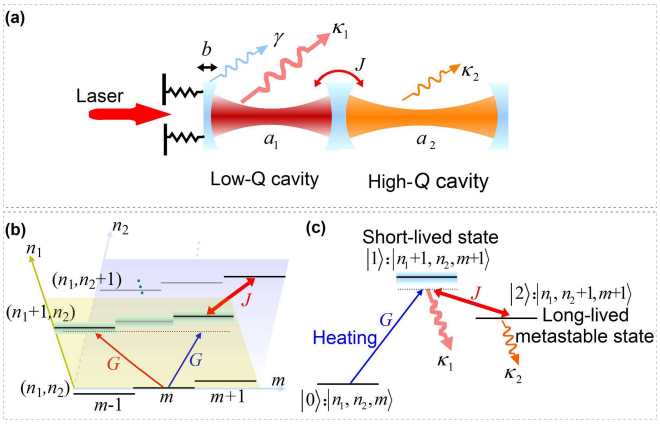

FIG. 1: (color online) (a) Fabry-Pérot equivalent of the current system with two coupled optical cavities. The first cavity is a low-Q cavity and the second cavity is a high-Q cavity. The mechanical mode only interact with the first cavity mode. (b) Energy level diagram of the system in the displaced frame. $|n_1, n_2, m\rangle$ denotes the state of n_1 photons in mode a_1, n_2 photons in mode a_2 and m phonons in mode b. The red double arrow denotes the coupling between states $|n_1+1, n_2, m+1\rangle$ and $|n_1, n_2+1, m+1\rangle$ with coupling strength J. (c) Energy levels forming the three-level configuration.

*Electronic address: yfxiao@pku.edu.cn; URL: www.phy.pku.edu.cn/~yfxiao/index.html
†Electronic address: cww2014@columbia.edu

II. SYSTEM MODEL

Figure 1(a) illustrates two coupled optical cavities. The first primary cavity supports the optical mode a_1 (frequency ω_1, decay rate κ_1) and the mechanical mode b (frequency $\omega_{\rm m}$, decay rate γ) with single-photon optomechanical coupling strength g, while the second auxiliary cavity supports the optical mode a_2 (frequency ω_2, decay rate κ_2) and does not interact with the mechanical mode b. The interaction between the two optical modes is denoted by the tunnel-coupling parameter J [33, 48–55]. The continuous-wave input laser excites mode a_1 with driving strength Ω. In the frame rotating at input laser frequency $\omega_{\rm in}$, the system Hamiltonian reads $H = -\Delta_1 a_1^\dagger a_1 - \Delta_2 a_2^\dagger a_2 + \omega_{\rm m} b^\dagger b + g a_1^\dagger a_1 (b^\dagger + b) + (J a_1^\dagger a_2 + J^* a_2^\dagger a_1) + (\Omega^* a_1 + \Omega a_1^\dagger)$, where $\Delta_1 \equiv \omega_{\rm in} - \omega_1$ and $\Delta_2 \equiv \omega_{\rm in} - \omega_2$ are the detunings. After linearization, the multi-photon optomechanical coupling strength reads $G \equiv g\alpha_1$ with α_1 the average intracavity field of mode a_1.

The energy levels of the coupled system are depicted in Fig. 1(b), where a series of three-level configurations can be extracted. In Fig. 1(c), $|1\rangle$ represents a short-lived state with high decay rate κ_1, while $|2\rangle$ denotes a long-lived metastable state with a small decay rate κ_2. Destructive quantum interference occurs between the two different excitation pathways, from $|0\rangle \to |1\rangle$ directly and from $|0\rangle \to |1\rangle \to |2\rangle \to |1\rangle$ indirectly. This allows the heating process through the optical field to be potentially suppressed. Meanwhile, the cooling process is almost unaffected due to off-resonance interaction.

III. COOLING THROUGH COUPLED CAVITY INTERACTIONS BEYOND THE RESOLVED SIDEBAND LIMIT

To demonstrate the cooling, we derive and calculate the spectral density of the optical force using the quantum noise approach (see Appendix B)

$$S_{FF}(\omega) = \frac{|G|^2 \kappa_1}{x_{\rm ZPF}^2} |\chi(\omega)|^2 \left[1 + \frac{\kappa_2}{\kappa_1} |J|^2 |\chi_2(\omega)|^2\right], \quad (1)$$

where $x_{\rm ZPF}$ is the zero-point mechanical fluctuation, $\chi^{-1}(\omega) = \chi_1^{-1}(\omega) + J^2\chi_2(\omega)$, $\chi_1^{-1}(\omega) = -i(\omega + \Delta_1') + \kappa_1/2$, $\chi_2^{-1}(\omega) = -i(\omega + \Delta_2) + \kappa_2/2$ and $\Delta_1' = \Delta_1 + 2|G|^2/\omega_{\rm m}$ is the optomechanical-coupling modified detuning. Without the second optical mode a_2, the noise spectrum reduces to $S_{FF}^{(J=0)}(\omega) = |G|^2 \kappa_1 |\chi_1(\omega)|^2 / x_{\rm ZPF}^2$, a Lorentzian noise spectrum. In the presence of mode a_2, $S_{FF}(\omega)$ becomes a complex lineshape due to interaction of the two optical modes. In Figs. 2(a) and 2(b) we plot the noise spectrum $S_{FF}(\omega)$ in the highly unresolved sideband regime $\kappa_1/\omega_{\rm m} = 10^4$ by examining various detunings Δ_1'. An asymmetric Fano (interference of a resonant scattering with continuum background) [56] lineshape or a symmetric narrow electromagnetically-induced transparency (EIT, interference of two resonant scattering or optical transitions) [57–60] lineshape appears with sharp spectral change compared with the low-Q spectral background. This greatly increases the asymmetry between cooling and heating processes, with potential for enhanced cooling rate $A_- \equiv S_{FF}(\omega_{\rm m}) x_{\rm ZPF}^2$ and suppressed heating rate $A_+ \equiv S_{FF}(-\omega_{\rm m}) x_{\rm ZPF}^2$. Here A_- (A_+) represents the rate for absorbing (emitting) a phonon by the intracavity field, as illustrated in Fig. 2(c) and 2(d). In the single cavity highly unresolved sideband regime, the cooling rate A_- and heating rate A_+ are almost the same, with net cooling rate $\Gamma_{\rm opt} \equiv A_- - A_+$ near zero [Fig. 2(c) and 2(e)]. In the presence of the second optical mode a_2, the quantum interference results in large suppression of A_+ while A_- is almost unchanged, leading to a very large net cooling rate $\Gamma_{\rm opt}$ [Fig. 2(d) and 2(f)]. Moreover, we note that the classical cooling limit $n_{\rm f}^{\rm c}$ ($\simeq \gamma n_{\rm th}/\Gamma_{\rm opt}$) is largely lowered, relaxing the requirement for initial cryogenic pre-cooling, i.e., higher bath thermal phonon number $n_{\rm th}$ can be tolerated. Furthermore, the quantum limit $n_{\rm f}^{\rm q}$ ($\simeq A_+/\Gamma_{\rm opt}$) is significantly reduced, breaking the resolved sideband requirement of backaction cooling. For the single cavity case, the lowest achievable quantum limit, obtained for detuning $\Delta_1' = -\kappa_1/2$ in the unresolved sideband condition, is given by $\kappa_1/(4\omega_{\rm m})$. In the coupled cavity approach here, κ_1 is no longer a limit on the final phonon occupancy through cancellation of quantum backaction heating.

By solving the quantum master equation and employing the covariance approach (see Appendix C), exact numerical results are obtained, with an example time evolution of the mean phonon number presented in Fig. 2(g). In the presence of the second cavity the mean phonon occupancy is cooled from an initial 10^4 to below 1 even for highly unresolved sideband case $\kappa_1/\omega_{\rm m} = 10^4$, while in the absence of the second cavity, the mechanical motion cannot be cooled for such a large $\kappa_1/\omega_{\rm m}$.

Compared with the conventional single cavity cooling case, a significant difference here is that the input laser can be blue detuned. In the quantum noise approach, the positive slope of $S_{FF}(\omega)$ is used for cooling while the negative slope corresponds to heating. For single cavity setup, positive slope of $S_{FF}(\omega)$ only appears on the left wing of the Lorentzian; while for coupled cavity system, the Fano or EIT spectrum has rich structures. For example, the EIT lineshape can be viewed as an inverse Lorentzian lineshape. In Fig. 3(a) we plot exact numerical results of the steady-state final phonon number $n_{\rm f}$ as a function of two detunings Δ_1' and Δ_2 for fixed inter-cavity interaction strength J. It shows optimal detunings are approximately described by $\Delta_1'(\Delta_2 + \omega_{\rm m}) = J^2$ (blue solid curve), calculated from Eq. (1) by maximizing the cooling rate A_-. In Figs. 3(b)-3(d) we plot $n_{\rm f} = n_{\rm f}^{\rm q} + n_{\rm f}^{\rm c}$, the quantum part $n_{\rm f}^{\rm q}$ and classical part $n_{\rm f}^{\rm c}$ as functions of Δ_1' and Δ_2 for optimized inter-cavity interaction tuned by $J = \sqrt{\Delta_1'(\Delta_2 + \omega_{\rm m})}$ [along the blue solid curve in Fig. 3(a)]. It shows that ground state cooling can be achieved for broad range of detunings. For the first cavity, this range exceeds $5\times10^4\omega_{\rm m}$; for the second cavity, significant cooling can be realized in the span of $-0.5 < \Delta_2/\omega_{\rm m} < 1$. In Fig. 3(c) the quantum limit $n_{\rm f}^{\rm q}$ minimum is obtained for large Δ_1' and negative Δ_2 (for Fano-like lineshapes), from a small quantum backaction heating $\propto S_{FF}(-\omega_{\rm m})$. On the other hand, the classical limit $n_{\rm f}^{\rm c}$ minimum is achieved for small Δ_1' and pos-

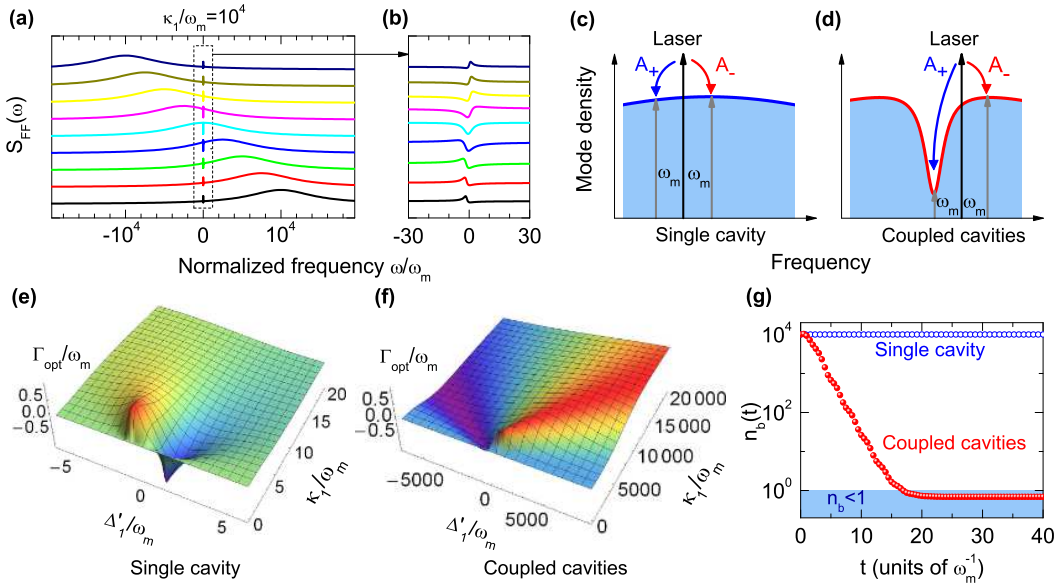

FIG. 2: (color online) (a) Optical force spectrum $S_{FF}(\omega)$ for $\kappa_1/\omega_{\rm m}=10^4$ and various Δ_1'. From top to bottom, Δ_1' decrease from κ_1 to $-\kappa_1$ with step $0.25\kappa_1$. (b) Zoom-in view of central one-fortieth of the dashed-box region in (a). (c) and (d): Frequency domain interpretation of optomechanical interactions with a single cavity (c) and coupled cavities (d). The black vertical arrows denote the input laser, the gray vertical arrows denote the scattering sidebands, and the red (blue) arrows denote the anti-Stokes (Stokes) scattering processes A_- (A_+). (e) and (f): Net optical cooling rate $\Gamma_{\rm opt}$ as functions of Δ_1' and κ_1 for a single cavity (e) and coupled cavities (f). (g) Exact numerical results of the mean phonon number $n_b(t)$ for coupled cavities (red closed circles) with $\Delta_1'=J^2/(\Delta_2+\omega_{\rm m})$. The single cavity case ($J=0$) with $\Delta_1'=-\kappa_1/2$ and $G/\omega_{\rm m}=10$ is plotted for comparison (blue open circles). The shaded region denotes $n_b<1$. Other unspecified parameters are $\kappa_1/\omega_{\rm m}=10^4$, $\kappa_2/\omega_{\rm m}=1$, $\Delta_2/\omega_{\rm m}=0.5$, $J=\sqrt{\kappa_1\omega_{\rm m}}$, $G=0.5J$, $\gamma/\omega_{\rm m}=10^{-5}$ and $n_{\rm th}=10^4$.

itive Δ_2 near $\Delta_2/\omega_{\rm m}\sim 1$ (for EIT-like lineshapes), which leads to a large cooling rate $\propto S_{FF}(\omega_{\rm m})$. The balance between these two limits lead to an optimal $\Delta_1'/\kappa_1\sim 3$ and $\Delta_2/\omega_{\rm m}\sim 0.3$ for the parameters in Fig. 3(b).

Figures 3(e) and 3(f) demonstrates the broad parameter space for ground state cooling in the unresolved sideband limit. With optimized couplings J and G, the final phonon number $n_{\rm f}$ for different ratios $\kappa_1/\omega_{\rm m}$ up to 10^6 are almost the same, which reveals that, arising from the unique interferences, the first cavity decay only acts as a background and have negligible influence on cooling for such large optical damping case. Figure 3(f) shows that for $\kappa_2/\omega_{\rm m}=0.5$, the tolerable initial bath phonon number $n_{\rm th}$ is up to 3×10^4 (green triangles), corresponding to $T=288$ K for $\omega_{\rm m}/2\pi=200$ MHz, readily available in physical measurements.

IV. EFFECTIVE DARK-MODE INTERACTIONS: ANALYTICAL COOLING LIMITS, STRONG COUPLING AND DYNAMICAL STABILITY

A. Analytical cooling limits

To gain more physical insights into the coupled cavity optomechanical system, we analyze the eigenmodes of the system. For large detuning , two of the system's eigenmodes are linear combinations of the mechanical mode and the high-Q cavity mode a_2, i.e., they are dark modes with respect to the low-Q cavity mode a_1. This dark mode doublet can be considered as a result of the effective interaction between the mechanical mode and the high-Q mode a_2. The interaction is concisely described by the effective parameters (see Appendix D)

$$|G_{\rm eff}|=\eta\,|G|\,,\ \kappa_{\rm eff}=\kappa_2+\eta^2\kappa_1,\ \Delta_{\rm eff}=\Delta_2-\eta^2\Delta_1',\quad (2)$$

where η is the scaled inter-cavity coupling strength given by

$$\eta=\frac{|J|}{|\Delta_1'|}\quad (3)$$

for large detuning $|\Delta_1'|>\kappa_1$. Note that mode a_2 does not directly interact with mode b, and the indirect effective interaction is mediated by mode a_1 [Fig. 4(a) inset]. It reveals from Eq. (2) that the effective detuning $\Delta_{\rm eff}$ is a combination of Δ_1' and Δ_2, uniquely allowing blue detuned Δ_1' and Δ_2 to obtain a red detuned $\Delta_{\rm eff}$. With the effective dark-mode interaction model, the cooling limits can be analytically described by (see Appendix D)

$$n_{\rm f}^{\rm eff}=\frac{\gamma n_{\rm th}}{\Gamma_{\rm eff}}+\frac{\kappa_{\rm eff}^2}{16\omega_{\rm m}^2},\quad (4)$$

where $\Gamma_{\rm eff}=4\,|G_{\rm eff}|^2/\kappa_{\rm eff}$ is the effective cooling rate. It reveals that ground state cooling requires $\kappa_2+\eta^2\kappa_1\lesssim 4\omega_{\rm m}$, only slightly dependent on the first cavity decay rate κ_1 for $\eta\ll 1$. The ultimate limitation is the second cavity decay rate

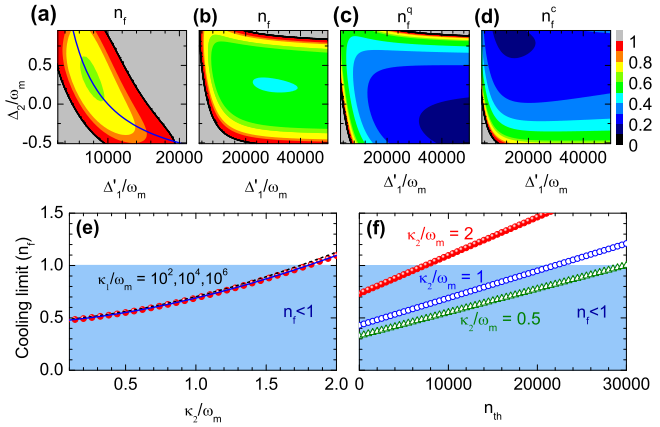

FIG. 3: (color online) (a) Exact numerical results of the final phonon number $n_{\rm f}$ as functions of $\Delta_1'/\omega_{\rm m}$ and $\Delta_2/\omega_{\rm m}$ for $J/\omega_{\rm m} = 100$, $G = 0.5J$. The blue curve corresponds to $\Delta_1'(\Delta_2+\omega_{\rm m}) = J^2$. (b)-(d): Final phonon number $n_{\rm f}$ (b), its quantum part $n_{\rm f}^{\rm q}$ (c) and classical part $n_{\rm f}^{\rm c}$ (d) as functions of $\Delta_1'/\omega_{\rm m}$ and $\Delta_2/\omega_{\rm m}$ for $J = \sqrt{\Delta_1'(\Delta_2+\omega_{\rm m})}$ and $G = 0.5J$. In (a)-(d), $\kappa_1/\omega_{\rm m} = 10^4$ and $n_{\rm th} = 10^4$. The black curves denote that the phonon number is 1. (e) and (f): Final phonon number $n_{\rm f}$ as a function of $\kappa_2/\omega_{\rm m}$ (e) and $n_{\rm th}$ (f). In (e), $n_{\rm th} = 10^4$, $\kappa_1/\omega_{\rm m} = 10^6$ (red closed circles), 10^4 (blue solid curve) and 10^2 (black dashed curve); in (f), $\kappa_1/\omega_{\rm m} = 10^4$, $\kappa_2/\omega_{\rm m} = 2$ (red closed circles), 1 (blue open circles) and 0.5 (green triangles). Other unspecified parameters are $J = \sqrt{\kappa_1\omega_{\rm m}}$, $G = 0.5J$, $\Delta_2/\omega_{\rm m} = 0.5$, $\Delta_1' = J^2/(\Delta_2+\omega_{\rm m})$ and $\gamma/\omega_{\rm m} = 10^{-5}$. The shaded regions denote $n_{\rm f} < 1$.

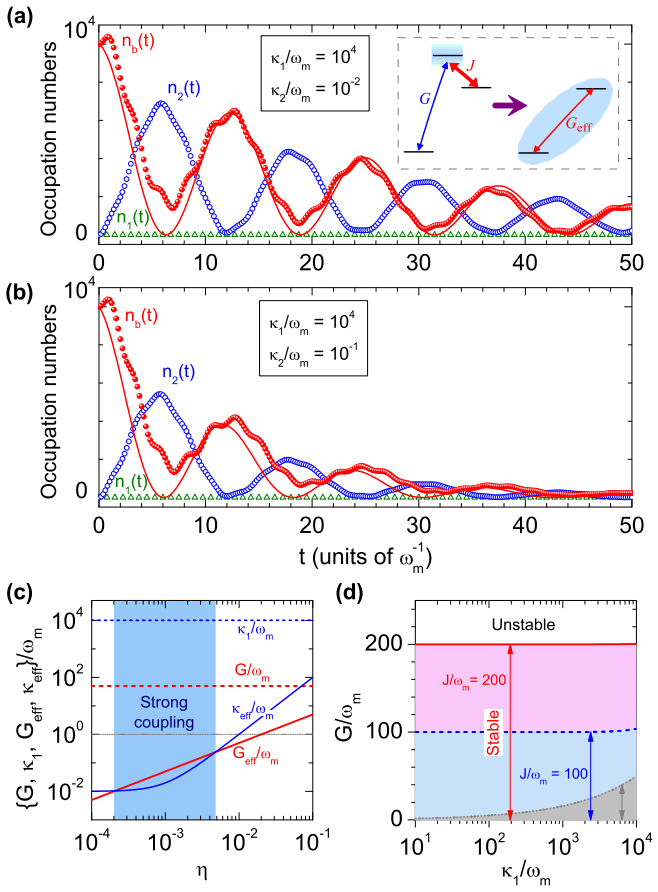

FIG. 4: (color online) Exact numerical results of the mean phonon number $n_b(t)$ (red closed circles), mean photon numbers $n_2(t)$ (blue open circles), $n_1(t)$ (green triangles) for $\kappa_1/\omega_{\rm m} = 10^4$, $J/\omega_{\rm m} = 200$ and $G = 0.5J$. In (a), $\kappa_2/\omega_{\rm m} = 0.01$; In (b), $\kappa_2/\omega_{\rm m} = 0.1$. The red solid curves are the analytical result for $n_b(t)$. Inset of (a): Schematic energy diagram of the effective dark-mode interaction. (c) Parameters $G/\omega_{\rm m}$ (red dashed curve), $\kappa_1/\omega_{\rm m}$ (blue dashed curve), $G_{\rm eff}/\omega_{\rm m}$ (red solid curve) and $\kappa_{\rm eff}/\omega_{\rm m}$ (blue solid curve) as functions of η. The shaded region denotes $G_{\rm eff} > \kappa_{\rm eff}$. The grey dotted line denotes the value of 1 in the unit of $\omega_{\rm m}$. (d) Dynamical stable regions for coupled cavities with $J/\omega_{\rm m} = 200$ (below the red solid curve) and $J/\omega_{\rm m} = 100$ (below the blue dashed curve), and single cavity case (below the gray dash-dotted curve). Other unspecified parameters are $\Delta_2/\omega_{\rm m} = -0.5$, $\Delta_1' = J^2/(\Delta_2+\omega_{\rm m})$, $\gamma/\omega_{\rm m} = 10^{-5}$ and $n_{\rm th} = 10^4$. This parameter regime can be reached, for example, in coupled microtoroids with $\omega_{\rm m} = 100$ MHz, $J = 20$ GHz, $\kappa_2 = 1 \sim 10$ MHz [33].

κ_2, which should be comparable to $\omega_{\rm m}$. Notably, since b is not directly couple to a_2, the optical and mechanical properties of the whole system can be optimized individually, without simultaneous requirements in the same resonator. Particularly, the second cavity does not need to support any mechanical modes, and the only requirement is relatively high optical Q.

B. Strong coupling

The current system also enables strong coupling between mode a_2 and mode b even when mode a_1 is highly dissipative, with the similar mechanism of strong-coupling cavity quantum electrodynamics in highly dissipative cavities [61]. Figure 4(a) and 4(b) shows that Rabi oscillation occurs for modes a_2 and b with $\kappa_1/\omega_{\rm m} = 10^4$. It reveals reversible energy exchange between these two indirectly coupled modes, with decoherence time much longer than the coherent exchange period. Note that the analytical results (red solid curve) calculated from the effective dark-mode interaction model (see Appendix D) agrees well with the exact numerical results. In this case the effective strong coupling condition $|G_{\rm eff}| > \kappa_{\rm eff}$ is satisfied. As shown in Eq. (2) and Fig. 4(c), for $\eta \ll 1$, both the effective coupling strength $|G_{\rm eff}|$ and effective cavity decay rate $\kappa_{\rm eff}$ are smaller than the original $|G|$ and κ_1, respectively. However, $\kappa_{\rm eff}$ decreases more rapidly than $|G_{\rm eff}|$ for decreasing η. Therefore, strong coupling regime can be reached, corresponding to the shaded region in Fig. 4(c).

From Eq. (2), it can be obtained that the strong coupling condition is relaxed to $|G| > 4\kappa_1\kappa_2$. For parameters examined in Fig. 4(a), we obtain $\eta = 2.5\times10^{-3}$, $G_{\rm eff}/\omega_{\rm m} = 0.25$, $\kappa_{\rm eff}/\omega_{\rm m} = 0.07$ and $\Delta_{\rm eff}/\omega_{\rm m} = -1$. With $n_{\rm th} = 2\times10^4$, we find $G_{\rm eff} > (\kappa_{\rm eff}, \gamma n_{\rm th})$, which is in the quantum-coherent coupling regime. This establishes an efficient quantum interface between the mechanical resonator and the photons, and allows the control of the mechanical quantum states.

C. Dynamical stability

To examine the dynamical stability of the coupled-mode optomechanical interactions, we calculate the stable regions through the Routh-Hurwitz criterion (see Appendix E) as presented in Fig. 4(d). It reveals that large optomechanical coupling G can be allowed to keep the system in the stable region, and it is more stable than the single cavity case, because the inter-cavity coupling provides additional restoring force to the mechanical oscillator. With the large allowed $|G|$, the effective coupling strength $|G_{\rm eff}|$ far exceeds the effective decay rate $\kappa_{\rm eff}$, bringing the system deeply in the strong coupling regime.

V. CONCLUSIONS

In summary, we have proposed the harnessing of coupled cavity interferences and dark mode interaction for ground state cooling of mechanical resonators and strong quantum-coherent optomechanical coupling beyond the resolved sideband limit. Through destructive quantum interferences, we demonstrate that the coupled cavity system not only significantly accelerates the cooling process, but also dramatically reduces the cooling limits. Ground state cooling is achievable for large cavity decay rate κ_1 when the coupled auxiliary cavity has modest decay rate $\kappa_2 \sim \omega_{\rm m}$. The auxiliary cavity mode is not directly coupled to the mechanical mode, allowing individual optimization of the optical and mechanical properties. Therefore, the first cavity only need to possess good mechanical properties while the second cavity only need to possess relatively high optical Q. Unlike the dissipative coupling mechanism [16, 17], we use pure dispersive coupling and all-optical EIT effect to realize destructive interference, and the interference comes from two resonant contributions. Note that the cavity decay rate in our case is the total decay rate where the intrinsic decay rate has been taken into account. This is important because in real experiments the external decay rate is usually tunable while the intrinsic cavity decay rate is the fundamental limitation. Different from the proposal using two-level atomic ensembles [23] and precooled atoms [25], our approach makes use of pure cavity optomechanical cooling effect arising from dynamical backaction, and it is quite practical in experimental realization, for instance, in a photonic crystal cavity system with highly unresolved sideband condition [62]. With dark-mode interaction in the strong coupling regime, the coupled cavity system allows for quantum-coherent coupling between mechanical mode and auxiliary cavity modes, with potential for quantum network applications [63–65]. This system establishes an efficient quantum interface between indirectly-coupled and individually-optimized mechanical resonators and optical cavities, which opens up the possibility for application of cavity quantum optomechanics beyond the resolved sideband regime, addressing the restricted experimental bounds at present.

Acknowledgments

We thank Jing Shu and Zhang-qi Yin for discussions. This work was supported by DARPA ORCHID program (C11L10831), 973 program (No. 2013CB328704, No. 2013CB921904), NSFC (Nos. 61435001, 11474011, 11222440, and 11121091), and RFDPH (No. 20120001110068).

Appendix A: System Hamiltonian and quantum Langevin equations

The Hamiltonian of the coupled cavity system is given by

$$H = H_{\rm free} + H_{\rm o-m} + H_{\rm o-o} + H_{\rm drive}. \tag{A1}$$

The first term $H_{\rm free}$ represents the free Hamiltonian of the optical and mechanical modes, described by $H_{\rm free} = \omega_1 a_1^\dagger a_1 + \omega_2 a_2^\dagger a_2 + \omega_{\rm m} b^\dagger b$, where ω_1, ω_2 and $\omega_{\rm m}$ are the resonance frequencies of the first (or primary) cavity mode a_1, the second (or auxiliary) cavity mode a_2 and the mechanical mode b. The second term of Eq. (A1) ($H_{\rm o-m}$) describes the optomechanical interaction between the first cavity mode a_1 and the mechanical mode b, which is written as $H_{\rm o-m} = g a_1^\dagger a_1 (b^\dagger + b)$ [66], where g represents the single-photon optomechanical coupling strength. The third term of Eq. (A1) ($H_{\rm o-o}$) describes the coupling between the two cavity modes a_1 and a_2, with the Hamiltonian

$$H_{\rm o-o} = J a_1^\dagger a_2 + J^* a_2^\dagger a_1, \tag{A2}$$

where J describes the interaction strength [33, 48–55]. The last term of Eq. (A1) ($H_{\rm drive}$) describes the optical driving. Assume that the system is excited through simultaneous driving of the two cavity modes with the same input laser frequency $\omega_{\rm in}$. In this case the Hamiltonian is given by $H_{\rm drive} = (\Omega_1^* e^{i\omega_{\rm in} t} a_1 + \Omega_1 e^{-i\omega_{\rm in} t} a_1^\dagger) + (\Omega_2^* e^{i\omega_{\rm in} t} a_2 + \Omega_2 e^{-i\omega_{\rm in} t} a_2^\dagger)$, where $\Omega_1 = \sqrt{\kappa_1^{\rm ex} P_1/(\hbar\omega_{\rm in})} e^{i\phi_1}$ and $\Omega_2 = \sqrt{\kappa_2^{\rm ex} P_2/(\hbar\omega_{\rm in})} e^{i\phi_2}$ denote the driving strengths, P_1 (P_2) is the input power and ϕ_1 (ϕ_2) is the initial phase for the first (second) input laser, and $\kappa_1^{\rm ex}$ ($\kappa_2^{\rm ex}$) is the input-cavity coupling rate for mode a_1 (a_2). Alternatively, the system can also be excited through single-mode driving of either cavity mode, corresponding to $\Omega_1 = 0$ or $\Omega_2 = 0$. This only affects the mean intracavity field of the two cavity modes and the equilibrium position of the mechanical resonator, while the quantum fluctuations and thereby the linearized quantum Langevin equations (see below) remain the same.

In the frame rotating at the input laser frequency $\omega_{\rm in}$, the Hamiltonian is written as $H = -\Delta_1 a_1^\dagger a_1 - \Delta_2 a_2^\dagger a_2 + \omega_{\rm m} b^\dagger b + g a_1^\dagger a_1 (b^\dagger + b) + (J a_1^\dagger a_2 + J^* a_2^\dagger a_1) + (\Omega_1^* a_1 + \Omega_1 a_1^\dagger) + (\Omega_2^* a_2 + \Omega_2 a_2^\dagger)$, where $\Delta_1 \equiv \omega_{\rm in} - \omega_1$, $\Delta_2 \equiv \omega_{\rm in} - \omega_2$ are the detunings.

The quantum Langevin equations are given by

$$\dot{a}_1 = \left(i\Delta_1 - \frac{\kappa_1}{2}\right) a_1 - iga_1(b^\dagger + b) - iJa_2 - i\Omega_1 - \sqrt{\kappa_1}a_{\mathrm{in},1}, \quad \text{(A3)}$$

$$\dot{a}_2 = \left(i\Delta_2 - \frac{\kappa_2}{2}\right) a_2 - iJ^* a_1 - i\Omega_2 - \sqrt{\kappa_2}a_{\mathrm{in},2}, \quad \text{(A4)}$$

$$\dot{b} = \left(-i\omega_{\mathrm{m}} - \frac{\gamma}{2}\right) b - iga_1^\dagger a_1 - \sqrt{\gamma}b_{\mathrm{in}}, \quad \text{(A5)}$$

where $\kappa_1 \equiv \omega_1/Q_1$, $\kappa_2 \equiv \omega_2/Q_2$, and $\gamma \equiv \omega_{\mathrm{m}}/Q_{\mathrm{m}}$ are the decay rates of the modes a_1, a_2 and b, respectively; Q_1, Q_2 and Q_{m} are the corresponding quality factors; $a_{\mathrm{in},1}$, $a_{\mathrm{in},2}$ and b_{in} are the corresponding noise operators, which satisfy $\langle a_{\mathrm{in},1}(t)a_{\mathrm{in},1}^\dagger(t')\rangle = \langle a_{\mathrm{in},2}(t)a_{\mathrm{in},2}^\dagger(t')\rangle = \delta(t-t')$, $\langle a_{\mathrm{in},1}^\dagger(t)a_{\mathrm{in},1}(t')\rangle = \langle a_{\mathrm{in},2}^\dagger(t)a_{\mathrm{in},2}(t')\rangle = 0$, $\langle b_{\mathrm{in}}(t)b_{\mathrm{in}}^\dagger(t')\rangle = (n_{\mathrm{th}}+1)\delta(t-t')$ and $\langle b_{\mathrm{in}}^\dagger(t)b_{\mathrm{in}}(t')\rangle = n_{\mathrm{th}}\delta(t-t')$. Here n_{th} is the thermal phonon number given by $n_{\mathrm{th}}^{-1} = \exp(\frac{\hbar\omega_{\mathrm{m}}}{k_{\mathrm{B}}T}) - 1$, where T is the environmental temperature and k_{B} is Boltzmann constant.

Now we apply a displacement transformation $a_1 \to \alpha_1 + a_1$, $a_2 \to \alpha_2 + a_2$, $b \to \beta + b$, where α_1, α_2 and β are c-numbers denoting the displacements of the optical and mechanical modes. The quantum Langevin equations are rewritten as

$$\dot{a}_1 = \left(i\Delta_1' - \frac{\kappa_1}{2}\right) a_1 - ig\alpha_1(b^\dagger + b) - iga_1(b^\dagger + b) - iJa_2 - \sqrt{\kappa_1}a_{\mathrm{in},1}, \quad \text{(A6)}$$

$$\dot{a}_2 = \left(i\Delta_2 - \frac{\kappa_2}{2}\right) a_2 - iJ^* a_1 - \sqrt{\kappa_2}a_{\mathrm{in},2}, \quad \text{(A7)}$$

$$\dot{b} = \left(-i\omega_{\mathrm{m}} - \frac{\gamma}{2}\right) b - ig\left(\alpha_1^* a_1 + \alpha_1 a_1^\dagger\right) - iga_1^\dagger a_1 - \sqrt{\gamma}b_{\mathrm{in}}, \quad \text{(A8)}$$

with the optomechanical-coupling modified detuning $\Delta_1' = \Delta_1 - g(\beta^* + \beta)$. Under strong driving condition, the nonlinear terms $iga_1(b^\dagger + b)$ and $iga_1^\dagger a_1$ in the above equations are neglected. Then the quantum Langevin equations become linearized, and the linearized system Hamiltonian can be extracted as

$$H_L = -\Delta_1' a_1^\dagger a_1 - \Delta_2 a_2^\dagger a_2 + \omega_{\mathrm{m}} b^\dagger b + (Ga_1^\dagger + G^* a_1)(b^\dagger + b) + (Ja_1^\dagger a_2 + J^* a_2^\dagger a_1), \quad \text{(A9)}$$

where $G \equiv g\alpha_1$ is the coherent intracavity field enhanced optomechanical coupling strength.

Appendix B: Quantum noise approach

From Eq. (A9) we obtain the optical force acting on the mechanical resonator $F = -(G^* a_1 + Ga_1^\dagger)/x_{\mathrm{ZPF}}$, where $x_{\mathrm{ZPF}} \equiv \sqrt{\hbar/(2m_{\mathrm{eff}}\omega_{\mathrm{m}})}$ is the zero-point fluctuation and m_{eff} is the effective mass of the mechanical resonator. The quantum noise spectrum of the optical force is given by the Fourier transform of the autocorrelation function $S_{FF}(\omega) \equiv \int dt e^{i\omega t}\langle F(t)F(0)\rangle$.

In the frequency domain, the operators $\tilde{a}_1(\omega)$, $\tilde{a}_2(\omega)$ and $\tilde{b}(\omega)$ obey

$$-i\omega\tilde{a}_1(\omega) = \left(i\Delta_1' - \frac{\kappa_1}{2}\right)\tilde{a}_1(\omega) - iG\left[\tilde{b}^\dagger(\omega) + \tilde{b}(\omega)\right] - iJ\tilde{a}_2(\omega) - \sqrt{\kappa_1}\tilde{a}_{\mathrm{in},1}(\omega), \quad \text{(B1)}$$

$$-i\omega\tilde{a}_2(\omega) = \left(i\Delta_2 - \frac{\kappa_2}{2}\right)\tilde{a}_2(\omega) - iJ^*\tilde{a}_1(\omega) - \sqrt{\kappa_2}\tilde{a}_{\mathrm{in},2}(\omega), \quad \text{(B2)}$$

$$-i\omega\tilde{b}(\omega) = \left(-i\omega_{\mathrm{m}} - \frac{\gamma}{2}\right)\tilde{b}(\omega) - i\left[G^*\tilde{a}_1(\omega) + G\tilde{a}_1^\dagger(\omega)\right] - \sqrt{\gamma}\tilde{b}_{\mathrm{in}}(\omega). \quad \text{(B3)}$$

Then we obtain

$$\tilde{b}(\omega) \simeq \frac{\sqrt{\gamma}\tilde{b}_{\mathrm{in}}(\omega) - i\sqrt{\kappa_1}A_1(\omega) - \sqrt{\kappa_2}A_2(\omega)}{i\omega - i[\omega_{\mathrm{m}} + \Sigma(\omega)] - \frac{\gamma}{2}}, \quad \text{(B4)}$$

where we have neglected $\tilde{b}^\dagger(\omega)$ terms and

$$A_1(\omega) = G^*\chi(\omega)\tilde{a}_{\mathrm{in},1}(\omega) + G\chi^*(-\omega)\tilde{a}_{\mathrm{in},1}^\dagger(\omega), \quad \text{(B5)}$$

$$A_2(\omega) = J\left[G^*\chi(\omega)\chi_2(\omega)\tilde{a}_{\mathrm{in},2}(\omega) - G\chi^*(-\omega)\chi_2^*(-\omega)\tilde{a}_{\mathrm{in}2}^\dagger(\omega)\right], \quad \text{(B6)}$$

$$\Sigma(\omega) = -i|G|^2[\chi(\omega) - \chi^*(-\omega)], \quad \text{(B7)}$$

$$\chi(\omega) = \frac{1}{\frac{1}{\chi_1(\omega)} + |J|^2\chi_2(\omega)}, \quad \text{(B8)}$$

$$\chi_1(\omega) = \frac{1}{-i(\omega + \Delta_1') + \frac{\kappa_1}{2}}, \quad \text{(B9)}$$

$$\chi_2(\omega) = \frac{1}{-i(\omega + \Delta_2) + \frac{\kappa_2}{2}}, \quad \text{(B10)}$$

$$\chi_{\mathrm{m}}(\omega) = \frac{1}{-i(\omega - \omega_{\mathrm{m}}) + \frac{\gamma}{2}}, \quad \text{(B11)}$$

where $A_{1,2}(\omega)$ accounts for the contribution of the first and second cavities, $\Sigma(\omega)$ represents the optomechanical self energy, $\chi(\omega)$ is the total response function of the coupled cavities, $\chi_1(\omega)$, $\chi_2(\omega)$ and $\chi_{\mathrm{m}}(\omega)$ are the response functions of the first cavity, the second cavity and the mechanical mode. The optomechanical coupling induced mechanical frequency shift $\delta\omega_{\mathrm{m}}$ and damping Γ_{opt} are given by $\delta\omega_{\mathrm{m}} = \mathrm{Re}\Sigma(\omega_{\mathrm{m}})$ and $\Gamma_{\mathrm{opt}} = -2\,\mathrm{Im}\Sigma(\omega_{\mathrm{m}})$.

Using $F(\omega) = -[G^* a_1(\omega) + Ga_1^\dagger(\omega)]/x_{\mathrm{ZPF}}$, the spectral density of the optical force is obtained as

$$S_{FF}(\omega) = \frac{|G\chi(\omega)|^2}{x_{\mathrm{ZPF}}^2}\left[\kappa_1 + \kappa_2|J|^2|\chi_2(\omega)|^2\right]. \quad \text{(B12)}$$

This equation corresponds to Eq. (1) of the main text.

Appendix C: Quantum master equation and covariance approach

The quantum master equation of the system reads

$$\begin{aligned}\dot{\rho} = & i[\rho, H_L] + \frac{\kappa_1}{2}\left(2a_1\rho a_1^\dagger - a_1^\dagger a_1\rho - \rho a_1^\dagger a_1\right) \\ & + \frac{\kappa_2}{2}\left(2a_2\rho a_2^\dagger - a_2^\dagger a_2\rho - \rho a_2^\dagger a_2\right) \\ & + \frac{\gamma}{2}(n_{\rm th}+1)\left(2b\rho b^\dagger - b^\dagger b\rho - \rho b_1^\dagger b_1\right) \\ & + \frac{\gamma}{2}n_{\rm th}\left(2b^\dagger\rho b - bb^\dagger\rho - \rho bb^\dagger\right), \end{aligned} \tag{C1}$$

where H_L is the linearized system Hamiltonian given by Eq. (A9).

To calculate time evolutions of the mean phonon number $n_b(t) = \langle b^\dagger b\rangle(t)$, we need to determine the mean values of all the time-dependent second-order moments, $\langle a_1^\dagger a_1\rangle$, $\langle a_2^\dagger a_2\rangle$, $\langle b^\dagger b\rangle$, $\langle a_1^\dagger a_2\rangle$, $\langle a_1^\dagger b\rangle$, $\langle a_2^\dagger b\rangle$, $\langle a_1 a_2\rangle$, $\langle a_1 b\rangle$, $\langle a_2 b\rangle$, $\langle a_1^2\rangle$, $\langle a_2^2\rangle$, and $\langle b^2\rangle$, which are determined by a linear system of ordinary differential equations $\partial_t\langle\hat{o}_i\hat{o}_j\rangle = {\rm Tr}(\dot{\rho}\hat{o}_i\hat{o}_j) = \sum_{k,l}\eta_{k,l}\langle\hat{o}_k\hat{o}_l\rangle$, where $\hat{o}_i$, $\hat{o}_j$, $\hat{o}_k$ and $\hat{o}_l$ are one of the operators a_1, a_2, b, $a_1^\dagger$, $a_2^\dagger$ and $b_1^\dagger$, and $\eta_{k,l}$ are the corresponding coefficients determined by Eq. (C1) [22]. Initially, the mean phonon number is equal to the bath thermal phonon number, i. e., $\langle b^\dagger b\rangle(t=0) = n_{\rm th}$, and other second-order moments are zero. The numerical results in the main text are obtained by solving these differential equations.

Appendix D: Effective dark-mode interaction

The second cavity mode a_2 does not directly interact with the mechanical mode b. However, there exists indirect interaction between them, which is mediated by the first cavity mode a_1. From Eqs. (A6)-(A8), after neglecting the nonlinear terms, we obtain the formally integrated form for the operators as

$$\begin{aligned} a_1(t) = & a_1(0)\exp(i\Delta_1' t - \frac{\kappa_1}{2}t) + \exp(i\Delta_1' t - \frac{\kappa_1}{2}t) \\ & \times\int_0^t[-iGb(\tau) - iGb^\dagger(\tau) - iJa_2(\tau) - \sqrt{\kappa_1}a_{{\rm in},1}(\tau)]\exp(-i\Delta_1\tau + \frac{\kappa_1}{2}\tau)d\tau, \end{aligned} \tag{D1}$$

$$a_2(t) = a_2(0)\exp(i\Delta_2 t - \frac{\kappa_2}{2}t) + \exp(i\Delta_2 t - \frac{\kappa_2}{2}t)\int_0^t[-iJ^* a_1(\tau) - \sqrt{\kappa_2}a_{{\rm in},2}(\tau)]\exp(-i\Delta_2\tau + \frac{\kappa_2}{2}\tau)d\tau, \tag{D2}$$

$$b(t) = b(0)\exp(-i\omega_{\rm m}t - \frac{\gamma}{2}t) + \exp(-i\omega_{\rm m}t - \frac{\gamma}{2}t)\int_0^t[-iG^* a_1(\tau) - iGa_1^\dagger(\tau) - \sqrt{\gamma}b_{\rm in}(\tau)]\exp(i\omega_{\rm m}\tau + \frac{\gamma}{2}\tau)d\tau, \tag{D3}$$

Consider the effects of mode a_1 as perturbations, and solve Eqs. (D2) and (D3), we obtain

$$a_2(t) \simeq a_2(0)\exp(i\Delta_2 t - \frac{\kappa_2}{2}t) + A_{{\rm in},2}(t), \tag{D4}$$

$$b(t) \simeq b(0)\exp(-i\omega_{\rm m}t - \frac{\gamma}{2}t) + B_{\rm in}(t), \tag{D5}$$

where $A_{{\rm in},2}(t)$ and $B_{\rm in}(t)$ denote the noise terms. By plugging Eqs. (D4) and (D5) into Eq. (D1) and with the condition $|\Delta_1| \gg |\Delta_2|$, $\kappa_1 \gg (\kappa_2, \gamma)$ we obtain

$$\begin{aligned} a_1(t) \simeq & -\frac{iG\left[b(t) + b^\dagger(t)\right]}{-i\Delta_1 + \frac{\kappa_1}{2}} - \frac{iJa_2(t)}{-i\Delta_1 + \frac{\kappa_1}{2}} \\ & + a_1(0)\exp(i\Delta_1 t - \frac{\kappa_1}{2}t) + A_{{\rm in},1}(t), \end{aligned} \tag{D6}$$

where the noise term is denoted by $A_{{\rm in},1}(t)$. By neglecting the fast decaying term containing $\exp(-\kappa_1 t/2)$ and plugging the expression back to Eqs. (A7) and (A8), we compare the equations with the effective single cavity case and obtain

$$i\Delta_2 - \frac{\kappa_2}{2} + \frac{|J|^2}{i\Delta_1' - \frac{\kappa_1}{2}} \longleftrightarrow i\Delta_{\rm eff} - \frac{\kappa_{\rm eff}}{2}, \tag{D7}$$

$$\left|\frac{J^* G}{i\Delta_1' - \frac{\kappa_1}{2}}\right| \longleftrightarrow |G_{\rm eff}|, \tag{D8}$$

where $G_{\rm eff}$ is the effective coupling strength, $\kappa_{\rm eff}$ is the effective decay rate of the optical cavity mode and $\Delta_{\rm eff}$ is the effective detuning between the input light and the optical resonance. Then the indirect interaction between mode a_2 and mode b can be described by the effective parameters $|G_{\rm eff}| = \eta|G|$, $\kappa_{\rm eff} = \kappa_2 + \eta^2\kappa_1$ and $\Delta_{\rm eff} = \Delta_2 - \eta^2\Delta_1'$ with $\eta = |J|/[\Delta_1'^2 + (\kappa_1/2)^2]^{1/2} \simeq |J|/|\Delta_1'|$ for $|\Delta_1'| > \kappa_1$. These correspond to Eq. (2) and (3) of the main text.

From these effective parameters, we obtain the effective spectral density of optical force as

$$S_{FF}^{\rm eff}(\omega) = \frac{\kappa_{\rm eff}|G_{\rm eff}\chi_{\rm eff}(\omega)|^2}{x_{\rm ZPF}^2}, \tag{D9}$$

where we have defined the effective response function

$$\chi_{\rm eff}(\omega) = \frac{1}{-i(\omega + \Delta_{\rm eff}) + \frac{\kappa_{\rm eff}}{2}}. \tag{D10}$$

In Fig. 5 the comparison between $S_{FF}^{\rm eff}(\omega)$ [Eq. (B12)] and $S_{FF}^{\rm eff}(\omega)$ [Eq. (D9)] is displayed. It reveals that for the region near the Fano resonance, the effective optical force spectrum is a good approximation.

In the effective resolved sideband limit ($\omega_{\rm m} > \kappa_{\rm eff}$) and weak coupling regime ($\kappa_{\rm eff} > G_{\rm eff}$), the cooling limit reads

$$n_{\rm f}^{\rm eff} = \frac{\gamma n_{\rm th}}{\Gamma_{\rm eff}} + \frac{\kappa_{\rm eff}^2}{16\omega_{\rm m}^2}, \tag{D11}$$

where $\Gamma_{\rm eff} = 4\left|G_{\rm eff}\right|^2/\kappa_{\rm eff}$ is the effective cooling rate.

After eliminating mode a_1, the effective system Hamiltonian is given by

$$H_{\rm eff} = -\Delta_{\rm eff} a_2^\dagger a_2 + \omega_{\rm m} b^\dagger b + (G a_2^\dagger + G^* a_2)(b + b^\dagger), \tag{D12}$$

Then the quantum master equation reads

$$\begin{aligned}\dot{\rho} = & i[\rho, H_{\rm eff}] + \frac{\kappa_{\rm eff}}{2}\left(2a_2\rho a_2^\dagger - a_2^\dagger a_2\rho - \rho a_2^\dagger a_2\right) \\ & + \frac{\gamma}{2}(n_{\rm th}+1)\left(2b\rho b^\dagger - b^\dagger b\rho - \rho b^\dagger b\right) \\ & + \frac{\gamma}{2} n_{\rm th}\left(2b^\dagger\rho b - bb^\dagger\rho - \rho bb^\dagger\right).\end{aligned} \tag{D13}$$

By solving the differential equations of all the second-order moments relevant with modes a_2 and b [22, 67], we obtain the time evolution of the mean phonon number in the effective strong coupling regime ($|G_{\rm eff}| > \kappa_{\rm eff}$) as

$$\begin{aligned} n_b(t) \simeq & \, n_{\rm th}\exp\left(-\frac{\kappa_{\rm eff}}{2}t\right)\cos^2(G_{\rm eff}t) \\ & + \frac{\gamma n_{\rm th}}{\kappa_{\rm eff}} + \frac{8\left|G_{\rm eff}\right|^2 + \kappa_{\rm eff}^2}{16\omega_{\rm m}^2}.\end{aligned} \tag{D14}$$

The red dashed-dotted curves in Fig. 4(a) and 4(b) of the main text are plotted according to this expression. Note that $n_b(t\to\infty) = \gamma n_{\rm th}/\kappa_{\rm eff} + (8\left|G_{\rm eff}\right|^2 + \kappa_{\rm eff}^2)/(16\omega_{\rm m}^2)$ corresponds to the cooling limit in the strong coupling regime. In our plots $n_{\rm th} \gg n_b(t\to\infty)$, so in Eq. (D14) we just simply add $n_b(t\to\infty)$ to the damped oscillation parts $n_{\rm th}\exp\left(-\kappa_{\rm eff}t/2\right)\cos^2(G_{\rm eff}t)$. In this case $n_b(0) \simeq n_{\rm th}$ can be satisfied in Eq. (D14).

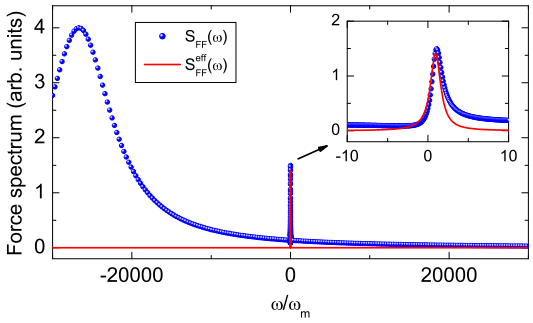

FIG. 5: Optical force spectrum $S_{FF}(\omega)$ (blue dots) and $S_{FF}^{\rm eff}(\omega)$ (red solid curve) for $\kappa_1/\omega_{\rm m} = 10^4$, $\kappa_2/\omega_{\rm m} = 1$, $\Delta_2/\omega_{\rm m} = 0.5$, $J/\omega_{\rm m} = 200$, $G = 0.5J$, $\Delta_1' = |J|^2/(\Delta_2+\omega_{\rm m})$, $\gamma/\omega_{\rm m} = 10^{-5}$ and $n_{\rm th} = 10^4$. The inset is a zoom-in view of the Fano region.

Appendix E: Dynamical stability condition

For single cavity case, the dynamical stability condition is given by

$$\Delta_1'\left[16\Delta_1'\left|G\right|^2 + (4\Delta_1'^2 + \kappa_1^2)\omega_{\rm m}\right] < 0, \tag{E1}$$

which is calculated from the Routh-Hurwitz criterion [68]. In the resolved sideband regime, for $\Delta_1' = -\kappa_1/2$, inequality (E1) reduces to

$$\left|G\right|^2 < \frac{\kappa_1\omega_{\rm m}}{4}. \tag{E2}$$

For the coupled cavity case, with the now derived effective parameters, the dynamical stability condition reads $\Delta_{\rm eff}[16\Delta_{\rm eff}\left|G_{\rm eff}\right|^2 + (4\Delta_{\rm eff}^2 + \kappa_{\rm eff}^2)\omega_{\rm m}] < 0$. Assume that the effective optomechanical interaction is in the resolved sideband regime, with the detuning $\Delta_{\rm eff} = -\omega_{\rm m}$, the stability condition reduces to $\left|G_{\rm eff}\right|^2 < \omega_{\rm m}^2/4 + \kappa_{\rm eff}^2/16$, which corresponds to

$$\left|G\right|^2 < \frac{4\omega_{\rm m}^2 + \left(\kappa_2 + \eta^2\kappa_1\right)^2}{16\eta^2}. \tag{E3}$$

Define the right-hand side of the inequality as S, then the minimum value of S is given by

$$S_{\rm min} = \frac{\kappa_1}{4}\sqrt{\omega_{\rm m}^2 + \frac{\kappa_2^2}{4}} + \frac{\kappa_1\kappa_2}{8}, \tag{E4}$$

which is obtained when $\eta = \eta_{\rm min} \equiv \sqrt[4]{4\omega_{\rm m}^2+\kappa_2^2}/\sqrt{\kappa_1}$. It reveals that, for the coupled cavity system, even in the worst case it allows larger optomechanical coupling to keep the system in the stable region, compared with the single cavity system for $\Delta_1' = -\kappa_1/2$ [inequality (E2)]. In Fig. 4(d) of the main text, the gray shaded region is plotted according to inequality (E2), the blue and red shaded regions denote inequality (E3) for $J/\omega_{\rm m} = 100$ and 200, respectively.

[1] T. Carmon, H. Rokhsari, L. Yang, T. J. Kippenberg, and K. J. Vahala, Phys. Rev. Lett. **94**, 223902, (2005).

[2] T. J. Kippenberg, H. Rokhsari, T. Carmon, A. Scherer, and K. J. Vahala, Phys. Rev. Lett. **95**, 033901, (2005).

[3] T. J. Kippenberg and K. J. Vahala, Science **321**, 1172 (2008).

[4] M. Aspelmeyer, T. J. Kippenberg, F. Marquardt, Rev. Mod. Phys. **86**, 1391 (2014).

[5] Y.-C. Liu, Y.-W. Hu, C. W. Wong and Y.-F. Xiao, Chin. Phys. B **22**, 114213 (2013).

[6] Y.-C. Liu and Y.-F. Xiao, Natl. Sci. Rev. doi: 10.1093/nsr/nwu050 (2014).

[7] J. D. Teufel, T. Donner, D. Li, J. W. Harlow, M. S. Allman, K. Cicak, A. J. Sirois, J. D. Whittaker, K. W. Lehnert, and R. W. Simmonds, Nature (London) **475**,359 (2011).

[8] J. Chan, T. P. Mayer Alegre, A. H. Safavi-Naeini, J. T. Hill, A. Krause, S. Gröblacher, M. Aspelmeyer, and O. Painter, Nature (London) **478**, 89 (2011).

[9] S. Gigan, H. R. Böhm, M. Paternostro, F. Blaser, G. Langer, J. B. Hertzberg, K. C. Schwab, D. Bäuerle, M. Aspelmeyer, and A. Zeilinger, Nature (London) **444**, 67 (2006).

[10] O. Arcizet, P.-F. Cohadon, T. Briant, M. Pinard, and A. Heidmann, Nature (London) **444**, 71 (2006).

[11] A. Schliesser, R. Rivière, G. Anetsberger, O. Arcizet and T. J. Kippenberg, Nature Phys. **4**, 415 (2008).

[12] S. Gröblacher, J. B. Hertzberg, M. R. Vanner, G. D. Cole, S. Gigan, K. C. Schwab, and M. Aspelmeyer, Nature Phys. **5**, 485 (2009).

[13] Y.-S. Park and H. Wang, Nature Phys. **5**, 489 (2009).

[14] A. Schliesser, O. Arcizet, R. Rivère, G. Anetsberger and T. J. Kippenberg, Nature Phys **5**, 509 (2009).

[15] T. Rocheleau, T. Ndukum, C. Macklin, J. B. Hertzberg, A. A. Clerk, and K. C. Schwab, Nature (London) **463**, 72 (2010).

[16] F. Elste, S. M. Girvin, and A. A. Clerk, Phys. Rev. Lett. **102**, 207209 (2009).

[17] A. Xuereb, R. Schnabel, and K. Hammerer, Phys. Rev. Lett. **107**, 213604 (2011).

[18] Y. Li, L.-A. Wu, and Z. D. Wang, Phys. Rev. A **83**, 043804 (2011).

[19] J.-Q. Liao and C. K. Law, Phys. Rev. A **84**, 053838 (2011).

[20] X. Wang, S. Vinjanampathy, F. W. Strauch, and K. Jacobs, Phys. Rev. Lett. **107**, 177204 (2011).

[21] S. Machnes, J. Cerrillo, M. Aspelmeyer, W. Wieczorek, M. B. Plenio, and A. Retzker, Phys. Rev. Lett. **108**, 153601 (2012).

[22] Y.-C. Liu, Y.-F. Xiao, X. Luan, and C. W. Wong, Phys. Rev. Lett. **110,** 153606 (2013).

[23] C. Genes, H. Ritsch, and D. Vitali, Phys. Rev. A **80**, 061803(R) (2009).

[24] J. Restrepo, C. Ciuti, and I. Favero, Phys. Rev. Lett. **112**, 013601 (2014).

[25] B. Vogell, K. Stannigel, P. Zoller, K. Hammerer, M. T. Rakher, M. Korppi, A. Jöckel, and P. Treutlein, Phys. Rev. A **87**, 023816 (2013).

[26] A. Xuereb, T. Freegarde, P. Horak, and P. Domokos, Phys. Rev. Lett. **105**, 013602 (2010).

[27] I. Wilson-Rae, N. Nooshi, W. Zwerger, and T. J. Kippenberg, Phys. Rev. Lett. **99**, 093901 (2007).

[28] F. Marquardt, J. P. Chen, A. A. Clerk, and S. M. Girvin, Phys. Rev. Lett. **99**, 093902 (2007).

[29] Q. Lin, J. Rosenberg, D. Chang, R. Camacho, M. Eichenfield, K. J. Vahala and O. Painter, Nature Photon. **4,** 236 (2010).

[30] S. Weis, R. Rivière, S. Deléglise, E. Gavartin, O. Arcizet, A. Schliesser, T. J. Kippenberg*,* Science **330,** 1520 (2010).

[31] A. H. Safavi-Naeini, T. P. M. Alegre, J. Chan, M. Eichenfield, M. Winger, Q. Lin, J. T. Hill, D. E. Chang, O. Painter*,* Nature (London) **472,** 69 (2011).

[32] G. S. Agarwal and S. Huang, Phys. Rev. A **81,** 041803(R) (2010).

[33] I. S. Grudinin, H. Lee, O. Painter, and K. J. Vahala, Phys. Rev. Lett. **104**, 083901 (2010).

[34] M. Ludwig, A. H. Safavi-Naeini, O. Painter, and F. Marquardt, Phys. Rev. Lett. **109**, 063601 (2012).

[35] Y.-D. Wang and A. A. Clerk, Phys. Rev. Lett. **108**, 153603 (2012).

[36] L. Tian, Phys. Rev. Lett. **108**, 153604 (2012).

[37] S. Barzanjeh, M. Abdi, G. J. Milburn, P. Tombesi, and D. Vitali, Phys. Rev. Lett. **109**, 130503 (2012)

[38] Y.-D. Wang and A. A. Clerk, New J. Phys. **14**, 105010 (2012).

[39] T. F. Roque and A. Vidiella-Barranco, arXiv: 1401.3696

[40] J. T. Hill, A. H. Safavi-Naeini, J. Chan, and O. Painter, Nature Commun. **3,** 1196 (2012).

[41] Y. Liu, M. Davanco, V. Aksyuk, and K. Srinivasan, Phys. Rev. Lett. **110**, 223603 (2013).

[42] C. Dong, V. Fiore, M. C. Kuzyk, and H. Wang, Science **338,** 1609 (2012).

[43] S. Gröblacher, K. Hammerer, M. R. Vanner, and M. Aspelmeyer, Nature (London) **460**, 724 (2009).

[44] E. Verhagen, S. Deléglise, S. Weis, A. Schliesser, and T. J. Kippenberg, Nature (London) **482**, 63 (2012).

[45] T. A. Palomaki, J. W. Harlow, J. D. Teufel, R. W. Simmonds, and K. W. Lehnert, Nature (London) **495**, 210 (2013).

[46] J. M. Dobrindt, I. Wilson-Rae, and T. J. Kippenberg, Phys. Rev. Lett. **101**, 263602 (2008).

[47] W.-j. Gu and G.-x. Li, Phys. Rev. A **87**, 025804 (2013).

[48] I. S. Grudinin and K. J. Vahala, Opt. Express **17**, 14088 (2009).

[49] C. Zheng, X. Jiang, S. Hua, L. Chang, G. Li, H. Fan, and M. Xiao Opt. Express **20**, 18319 (2012).

[50] B. Peng, Ş. Kaya Özdemir, F Lei, F Monifi, M Gianfreda, G L Long, S Fan, F Nori, C. M. Bender, and L. Yang, Nature Phys. **10**, 394 (2014).

[51] Q. Xu, S. Sandhu, M. L. Povinelli, J. Shakya, S. Fan, and M. Lipson, Phy. Rev. Lett. **96**, 123901 (2006).

[52] Y.-F. Xiao, M. Li, Y.-C. Liu, Y. Li, X. Sun, and Q. Gong, Phys. Rev. A **82**, 065804 (2010).

[53] Y. Sato,Y. Tanaka, J. Upham, Y. Takahashi, T. Asano, and S. Noda, Nature Photon. **6**, 56 (2012).

[54] J. Cho, D. G.. Angelakis, and S. Bose, Phys. Rev. A **78**, 022323 (2008).

[55] B.-B. Li, Y.-F. Xiao, C.-L. Zou, X.-F. Jiang, Y.-C. Liu, F.-W. Sun, Y. Li, and Q. Gong, Appl. Phys. Lett. **100**, 021108 (2012).

[56] U. Fano, Phys. Rev. **124**, 1866 (1961).

[57] S. E. Harris, Phys. Rev. Lett. **62**, 1033 (1989).

[58] L. V. Hau, S. E. Harris, Z. Dutton, and C. H. Behroozi, Nature (London) **397**, 594 (1999).

[59] M. D. Lukin and A. Imamoğlu, Phys. Rev. Lett. **84**, 1419 (2000).

[60] M. Fleischhauer, A. Imamoglu, and J. P. Marangos, Rev. Mod. Phys. **77**, 633 (2005).

[61] Y.-C. Liu, X. L, H.-K. Li, Q. Gong, C. W. Wong, and Y.-F. Xiao, Phys. Rev. Lett. **112**, 213602 (2014)

[62] J. Zheng, Y. Li, M. S. Aras, A. Stein, K. L. Shepard, and C. W. Wong, Appl. Phys. Lett. **100**, 211908 (2012)

[63] K. Stannigel, P. Rabl, A. S. Sørensen, P. Zoller, and M. D.

Lukin, Phys. Rev. Lett. **105**, 220501 (2010).
[64] K. Stannigel, P. Rabl, A. S. Sørensen, M. D. Lukin and P. Zoller, Phys. Rev. A **84**, 042341 (2011).
[65] S. J. M. Habraken, K. Stannigel, M. D. Lukin, P. Zoller, and P. Rabl, New J. Phys. **14**, 115004 (2012).
[66] C. K. Law, Phys. Rev. A **51**, 2537 (1995).
[67] I. Wilson-Rae, N. Nooshi, J. Dobrindt, T. J. Kippenberg and W. Zwerger, New J. Phys. **10**, 095007 (2008).
[68] E. X. DeJesus and C. Kaufman, Phys. Rev. A **35,** 5288 (1987).